Article

A Molecular Simulation Approach to Bond Reorganization in Epoxy Resins: From Curing to Deformation and Fracture

Julian Konrad, Robert H. Meißner, Erik Bitzek, and Dirk Zahn*

Cite This: *ACS Polym. Au* 2021, 1, 165−174

Read Online

ACCESS | Metrics & More | Article Recommendations | Supporting Information

ABSTRACT: We model bond formation and dissociation processes in thermosetting polymer networks from molecular dynamics simulations. For this, a coarsened molecular mechanics model is derived from quantum calculations to provide effective interaction potentials that enable million-atoms scale simulations. The importance of bond (re)organization is demonstrated for (i) simulating epoxy resin formation—for which our approach leads to realistic network models which can now account for degrees of curing up to 98%. Moreover, (ii) we elucidate the competition of bond dissociation and bond reformation during plastic deformation and fracture. On this basis, we rationalize the molecular mechanisms that account for the irreversible nature of damaging epoxy polymers by mechanical load.

KEYWORDS: epoxy resin, reactive force-field, molecular dynamics, curing fracture, tensile testing
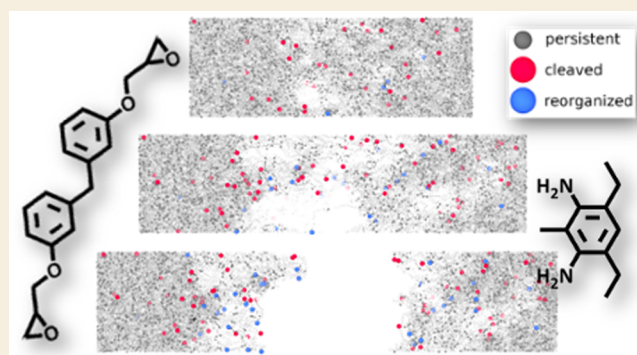
1. INTRODUCTION

Epoxy resins are widely used polymer materials featuring covalently bonded networks of at least two types of constituents.[1] The enormous industrial relevance of this class of compounds motivated an abundance of experimental studies of curing behavior and mechanical properties.[2−6] On the other hand, only a comparatively smaller number of molecular simulation studies have been performed for a deeper understanding of the underlying mechanisms.[7−16] A key hurdle to the atomic scale modeling of epoxy resins is given by the complexity of its network structure and thus the large and potentially multimillion atom systems required.[17] While practically no ordering is observed beyond the nanometer scale, local (atomic scale) arrangements are far from random and allow for almost 100% matching of bonding partners (experiments[18] indicate curing up to 99%). In the absence of full detail structure identification from crystallography, molecular simulation studies must either rely on "guessed" network structures or elucidate the curing process itself before addressing any characterization of mechanical properties.[14,16,19] The formation of epoxy networks is based on a cascade of linking events each based on bimolecular reactions of the epoxy compound (such as bisphenol A-diglycidylether) and amines used as multinary linker species. While individual linking reactions are thermally induced and in principle reversible, the overall binding network of the thermosetting polymer, however, forms in an irreversible manner. Indeed, with increasing degree of cross-linking, the initially mobile precursors are locked into a permanent network and the system evolves to a stiff epoxy resin. As a consequence, only the onset of thermoset curing is accessible to direct molecular dynamics (MD) or Monte Carlo (MC) simulation, and efficient protocols for assigning suitable binding partners are needed at later stages of network formation.[7,8,16,20,21] Despite ongoing progress, so far molecular simulation models still fall short of achieving the almost 100% degree of cross-linking that is reached in epoxy resins used in industrial applications.[18] The current benchmark of 93% cross-linking was obtained from a combined quantum mechanical/molecular mechanics approach that used smooth topology transfers[7,8] to facilitate network relaxation in the course of linking candidate pairs of reactants.[16] In that study, we focused the computationally demanding quantum calculations on individual linking reactions, while a Monte Carlo simulation type procedure is used to build an energetically favorable polymer network in a stepwise fashion. To this end, detailed balance, that is, the account of possible unlinking steps, could only be implemented for the explicit linking attempt under consideration. This ignores possible bond dissociation and reorganization at later stages of network formation. However, it is intuitive to expect that local corrections of the forming

polymer network may help to avoid internal stress.[21] As a consequence, molecular simulation protocols should ideally describe the reactivity of all epoxy moieties in a simultaneous manner. Unfortunately, this diminishes the performance of quantum mechanical/molecular mechanics approaches drastically, as practically the entire system must be described as the reactive species. As a consequence, reactive force-fields appear as the best option currently available to enable bonding/unbonding studies of >10,000-atom-sized polymer models from 100 ns scale molecular dynamics runs. Indeed, the most prominent interaction model of this kind, ReaxFF,[22] has already been employed to model epoxy resins—yet focusing on small models and short time scales, respectively.[23,24] ReaxFF aims at a full account of bond formation/dissociation, namely, the prediction of reaction energy and barriers at reasonable agreement with quantum chemical references.[25] This is a very worthwhile endeavor on its own. However, we argue that the specific problem of the self-organization of thermosetting polymer networks—and to quite some extent also the modeling of deformation and fracture processes—calls for a conceptually different type of reactive force-field. In what follows, we coarsen quantum chemically derived reaction profiles into a deliberately augmented reactive force-field. Our concept is to design interaction models to properly account for the energy change of polymer network linking/dissociation and to reproduce the maximum force needed for breaking epoxy bonds—but to artificially diminish the reaction barrier. From this, we provide drastic enhancements of the bonding and/or dissociation kinetics, thus extending the limited time scale of molecular simulation runs. In turn, our model shall reflect realistic energetics, including elastic properties and the yield stress for epoxy bond dissociation. Moreover, the versatility of our modeling approach is demonstrated in terms of studying thermoset curing, polymer deformation, and fracture.

2. METHODS AND MODELS

The quantum calculations were performed by Gaussian[26] at the B3LYP/6-311+G** level. Closed electron shell and (bi)radicalic states were implemented by assigning the spin multiplicity accordingly. For the MD simulations, the LAMMPS package (March 2020 version) was used with a simulation time step of 0.5 fs.[27] Constant temperature (0.1 ps) and pressure (1.0 ps) are implemented by the Nosé-Hoover algorithm. Coulombic interactions are described by the damped shifted force potential using a cutoff distance of 10 Å.[28] Molecular visualization and analyses were performed with VMD,[29] RStudio,[30] and GIMP.[31]

2.1. Interaction Models

Our thermosetting polymer model is based on the widely used bisphenol F-diglycidyl-ether (BFDGE) along with 3,5-diethyltoluene-2,4-diamine (DETDA) as the linker species (Figure 1, top left). Upon addition reactions of the epoxy and the amine groups, a branched network architecture is formed. In the fully cured epoxy resin, each $-NH_2$ moiety forms two links, and the underlying curing reaction can hence be divided into two classes (Figure 1). In the gas phase, quantum calculations indicate that both the single and double linking reactions are exothermic, namely, by $\Delta E_{single} = -25.5$ kcal/mol and $\Delta E_{double} = -15.5$ kcal/mol, respectively.

To assess energy profiles for these reactions, it is intuitive to focus on the C−N bond distances. However, the actual reaction coordinate is more complex, as the addition reaction of BFDGE and DETDA compounds involves a proton transfer from the amine to the epoxy group. The situation is even more complicated for the reverse reaction. During fracture of epoxy materials, the network may experience drastic deformation before actual bond dissociation. This can imply sterical hindering of the back-transfer of the proton such
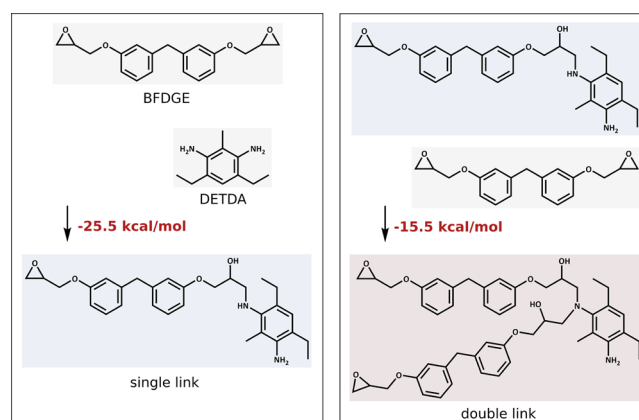

Figure 1. Bimolecular curing reactions based on BFDGE and DETDA pointing out the single link (left, most exothermic) and the double link (right) formation.

that some of the links may be forced to undergo biradicalic bond cleavage. Indeed, experiments could identify a traceable amount of radical formation during epoxy fracture.[32] Using analogous models and quantum approaches as for the single link formation,[16] we calculated the energy change for the C−N bond cleavage into biradicals. From this, a substantially larger dissociation energy of ∼65 kcal/mol (as compared to $-\Delta E_{single} = 25.5$ kcal/mol) was found. The extra cost of about 40 kcal/mol suggests that the fracture of epoxy networks should generally avoid the radicals mechanism, except for local configurations hampered by significant sterical hindering. Likewise, also biradicalic cleavage of C−C and C−O bonds (which feature even larger bond dissociation energies) should be a minor occurrence. In the following, we will therefore focus on nonradical routes of both C−N bond formation and dissociation. For this, a series of relaxed energy scans was performed using the C−N distance as descriptor of the reaction progress (Figure 2). In parallel runs, both protonation states were explored by fixing the proton either within the product-related OH group or to the amine. As starting points, the single linked molecule was prepared at the desired protonation state
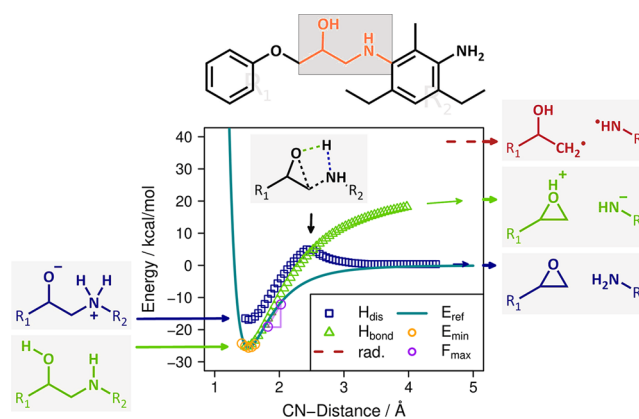
Figure 2. Energy profiles for single link dissociation/formation routes as functions of the C−N bond distance as obtained from quantum calculations. Within restraint structure optimization runs, both protonation states are explored, namely, by fixing the N−H bonds of the linker (blue curve) or by restraining the O−H bond of the linked species (green curve). Our reactive force-field model aims at reproducing the minimum energy route to C−N bonding/cleavage—however, deliberately "flattening" the reaction barrier. The fitted curve (cyan) is hence intended to reproduce only a small interval of the energy profile of the linked species (E_{min} and nearby data points, highlighted in orange), the maximum C−N binding force (purple) and the asymptotic behavior for distances beyond 4 Å.

and subjected to (unrestraint) geometry optimization. Next, the O−H and N−H bond distances were fixed according to the (local) energy minimum structures, and the molecules are subjected to relaxed energy scans at various C−N distances. On this basis, a rough estimate of the transition state is obtained at a C−N distance of about 2.5 Å and a barrier of 5 kcal/mol. This corresponds to C−N bond stretching much beyond the maximum in the restoring force F_{max} = 34.6 kcal/(mol Å) at 1.75 Å. However, for coarsening the linking/dissociation reaction we shall use an augmented energy profile that retains a series of key features while augmenting the reaction barrier. For the single link reaction, Figure 2 indicates the chosen data points to describe (i) the curvature of the minimum energy profile near the equilibrium C−N distance, (ii) the maximum force experienced during C−N bond elongation/formation, and (iii) the overall energy change of the linking reaction. The same concept is used for creating an augmented energy profile for the double link formation/dissociation reflecting its lower formation energy and correspondingly reduced pulling force needed for dissociation (SI Figure S1). On this basis, two simple C−N potential energy functions are obtained which reasonably reproduce the bulk properties of both reactant/product states and the energy change upon bond formation—hence enabling the modeling of polymer network linking. Moreover, by reproducing the maximum force needed for link dissociation our reactive force-field also allows for fracture modeling. On the other hand, the accurate account of the reaction barrier—a major challenge in ReaxFF[23]—is not even attempted. Instead, our coarse-grained model is designed for augmenting the reaction barrier such that the kinetics of both curing and plastic deformation/fracture are boosted in favor of more efficient molecular simulations. Molecular mechanics models of BFDGE and DEDTA, its single- and double-linked species as well as the entire epoxy resin are readily available, and the OPLS-AA force-field has already been approved to reproduce elastic properties[16] and glass transition characteristics. Moreover, by smooth transitions between the molecular topologies, we also demonstrated the molecular mechanics modeling of network relaxation during the linking of preselected bonding partners.[16] The key limitation of modeling bond formation in this manner is given by the change of interaction potentials in terms of both force field parameters such as bond distances, partial charges etc., and, more importantly, the assignment of intramolecular energy terms themselves. Thus, upon the addition/dissociation reaction, C−N bond formation and the proton transfer give rise to new bond, angle, and torsion potentials—if modeled by molecular mechanics at the atomic level of detail. In the following, we amend this computational limitation by coarsening the involved groups such that no more topology switching is needed during reactive molecular dynamics simulations. For this, a united atom concept is used to describe the hydrogen atoms of epoxy and amine moieties implicitly (Figure 3). This reduction of local detail is designed to also implement the proton transfer upon C−N bond formation/cleavage, thus universal O, C and N parameters are used to model epoxy/hydroxy oxygen and carbon atoms, as well as primary, secondary, and tertiary amines, respectively. On this basis, epoxy linking may be modeled by simple pairwise potentials between the coarsened O, C, and N interaction sites. To this end, we essentially use the topology of the unlinked species; however, the Lennard-Jones parameters and partial charges for the coarsened atoms (C_{cg}, O_{cg}, and N_{cg}) were taken as arithmetic averages of the OPLS-AA/UA values for the linked and unlinked species, respectively. By doing so, particular care is needed to maintain the C_{ep2}−C_{cg}−N_{cg} valence angles of the linked molecules. For this purpose, we add further interaction sites (is) next to the coarsened C and N moieties as indicated in Figure 3. The C_{ep2}−O_{cg}−$C_{cg/is}$ and $N_{cg/is}$−C_{ar} groups are each modeled as rigid units, respectively. The cg−is distances were chosen to be 0.6 Å, which is adopted from the modeling of electron lone-pairs in the OPLS-AA force-field. Likewise, the angle $\angle(C_{ep2}−C_{cg}−C_{is})$ was set to 120°, $\angle(C_{ar}−N_{cg}−N_{is})$ to 110°, and $\angle(O_{cg}−C_{cg}−C_{is})$ to 65°, respectively. While temporarily also fixing the C_{cg}−N_{cg} distance to the bond length of the linked molecule, additional C_{cg}−N_{is} and N_{cg}−C_{is} interaction potentials are derived to ensure the correct angle $\angle(N_{cg}$−C_{cg}−$C_{ep2})$ of 106°. For this, a short-ranged Lennard-Jones type
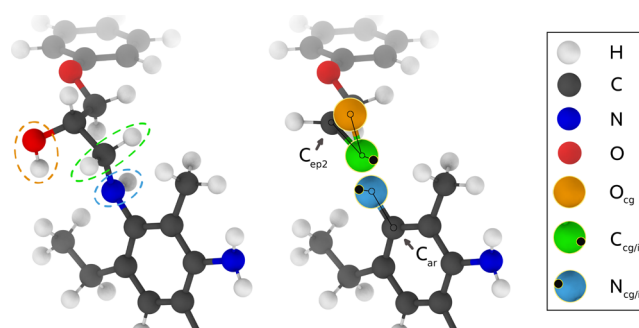
Figure 3. All-atom model (left, shown for the single linked molecule) is transferred to a coarse-grained (right) approach that implicitly describes the protonation states before and after epoxy linking. Note that the C−O_{cg}−C motif reflects the unreacted expoxy group, whereas the overall molecular alignment is that of the linked species. In the absence of multibody potentials between the epoxy and the amine moieties, the alignment of the linked molecules is maintained by additional C_{is} and N_{is} interaction sites, respectively. Moreover, the different binding energy of the single and double linking is reproduced from repulsive C_{cg}−C_{cg} potential energy terms.

potential energy function is chosen in order to not affect the orientation of yet unreacted epoxy and linker species. The best fit to the OPLS-AA topology of the linked molecule was obtained from a two-dimensional parameter screening of the dedicated C_{cg}−N_{is} and N_{cg}−C_{is} Lennard-Jones type potentials using 0.0001 kcal/mol and 3.0 Å as parameters for tuning binding energies and van-der-Waals radii, respectively. Note that no further interactions are considered for the N_{is} and C_{is} sites. Next, the C_{cg}−N_{cg} interaction potential is fitted to the described effective energy profile featuring augmented reaction barriers to enable linking/unlinking reactivity of our simulation models. For this purpose, a relaxed C_{cg}−N_{cg} energy scan is performed for the coarse-grained model (including the additional interaction sites) and a new potential is tabulated as the difference of this scan with respect to the reference illustrated in Figure 2. This reactive C_{cg}−N_{cg} potential is applied to both single and double linking; however, considering the lower formation energy of the second linking reaction by means of an additional C_{cg}−C_{cg} pair potential. The latter is directly tabulated to reproduce the augmented C−N bond cleavage profile for the double-linked species as illustrated in SI section S1. Consequently, all states ranging from the unlinked precursors to the cured resins are modeled at constant molecular topology (that of the precursors), while enabling linking reactions at realistic formation energy, maximal force needed for dissociation and ensuring proper molecular geometry of the links in the polymer network. The elaborated molecular topology, the tabulated interaction potentials, and the bulk epoxy models used for benchmarking can be made available as LAMMPS files upon request.

2.2. Simulation Systems

Two epoxy models λ of different sizes were explored, both using the ideal 2:1 ratio of BFDGE:DEDTA molecules. This first system λ_{ref} (256 + 128 molecules, cubic box of L_{box} = 4.3 nm after curing) is chosen in line with our earlier study as a reference, whereas the larger model λ_{large} counts 2048 + 1024 molecules (L_{box} = 8.4 nm after curing) of BFDGE and DEDTA, respectively. For both systems, we first prepared melts of the precursors (using the nonreactive OPLS-AA model) mimicked by 3D periodic boundary conditions. After 5 ns relaxation at 460 K and 1 atm, the simulation systems were subjected to the curing analyses as discussed in the Results section.

2.3. Protocols for Sampling Bulk Properties

After curing at 460 K, the bonded epoxy resin models were relaxed at ambient conditions to (i) explore the elastic properties and (ii) provide starting points for assessing the glass transition temperature T_G of the cured and relaxed epoxy models. For the latter, we first cooled to 100 K and then heated the system from 100 to 700 K at a

rate of 10 K/ns. Using the analog approach, we also first heated to 700 K and then cooled to 100 K. The glass transition temperature was then taken as the average of the values observed from the heating and cooling runs (Figure S2). The barostat (1 atm pressure) is allowed to change the simulation cell anisotropically, while the change of the overall density is monitored as the indicator for the glass transition. For the characterization of the elastic properties, the cured polymer models were subjected to 5 ns runs at 300 K and 1 atm, again allowing anisotropic cell variations. To account for their temperature-dependence, we sampled the elastic moduli from the fluctuations $\Delta\sigma$ of the volume V, cell dimensions l_x, l_y, and l_z, and cell vector angles ($\angle(x, y)$, $\angle(y, z)$, and $\angle(z, x)$), respectively. Using the linear response theory, the bulk K, Young's Y, and shear G modulus are computed from[16]

$$Y_x = \frac{k_B T}{(\Delta\sigma_{l_x})^2} \frac{\langle l_x \rangle^2}{\langle V \rangle} \qquad G_{xy} = \frac{k_B T}{(\Delta\sigma_{\angle(x,y)})^2 \langle V \rangle}$$

$$K = \frac{k_B T}{(\Delta\sigma_V)^2} \langle V \rangle$$

3. RESULTS AND DISCUSSION

3.1. Thermoset Curing

As the reactive FF modeling of epoxy linking/unliking is based on the augmented energy profile shown in Figure 1, we largely omit the reaction barrier of covalent bond reorganization. Indeed, the precursor liquid of BFDGE and DETDA molecules showed rapid (10 ps scale) linking reactions up to a degree of cross-linking of about 80% (Figure 4). Strikingly, only about
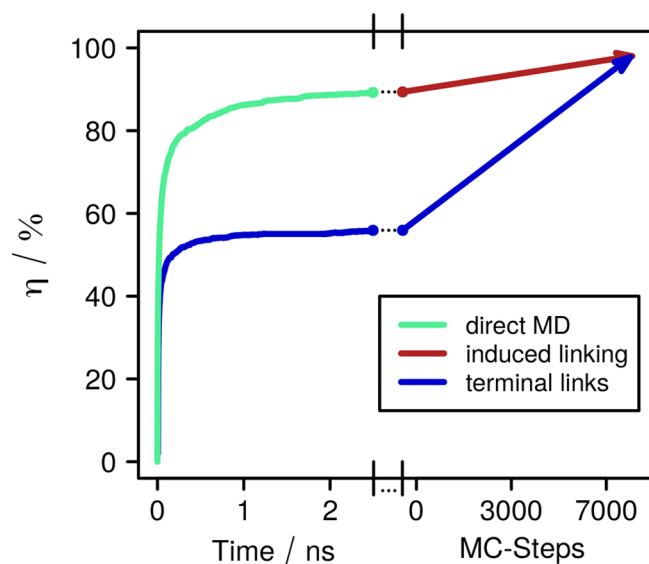
Figure 4. Cross-linking procedure using direct MD (green) and induced linking (red) by MC simulation. The blue curve indicates the percentage of terminal links, i.e., cross-links also found in the final polymer structure. The difference between the two curves indicates the level of bond rearrangements needed to reach networks of near 100% cross-linking.

half of these links prevail upon model propagation to the final degree of epoxy bonding. In other terms, our reactive FF leads to excessive curing kinetics (as desired) but also enables the rearrangement of epoxy links in favor of more compact resins. During nanosecond-scale reorganization observed from direct MD simulation, the degree of cross-linking steadily increases, however, approaching the desired 100% only logarithmically. For this reason, we adopted our recently developed MC

approach[16] to the curing of the present model (at 460 K and 1 atm as in ref 16). Likewise, each MC attempt refers to the testing of bond formation of nearby reaction partners—which are randomly picked among a candidate list created by a C−N distance criterion chosen as 5 Å. As the reactive FF does not require the switching of topologies for imposing bond formation, we simply used distance restraints for this purpose. The latter were implemented as linear ramping to the equilibrium C−N bond length within 10 ps MD runs. After inducing a specific epoxy bond in this manner, the system is propagated without the corresponding C−N distance restraint. As a consequence, each link is allowed to dissociate (and reorganize) during relaxation and, more importantly, during further attempts of bond formation. This reflects a significant extension of our previous MC approach which considered bond dissociation only in terms of the possibility of failed attempts in a given MC move.[16] Indeed, we find it is quite beneficial to allow all epoxy links to reorganize during the entire curing process rather than only rejecting endothermic linking of the specific candidates of a MC attempt. In Figure 4, we discriminate the overall degree of cross-linking from the percentage of persisting links with respect to the final polymer network. While the real kinetics of epoxy curing would be triggered by the reaction barriers of many linking steps happening in parallel, our approach artificially speeds up the polymerization. This comes at the price of "premature" linking which, however, is amended in an unbiased manner at later stages of the simulation. Within the limited time scales accessible to molecular simulations, we argue that the combination of the reactive FF with network refinement by MC simulations is particularly suited for efficient modeling of epoxy network formation. Indeed, we could boost the degree of cross-linking in the molecular simulation models up to $\eta = 98\%$ at still manageable computational costs (Table 1).

3.2. Bulk Properties

To benchmark our reactive FF, we first demonstrate consistence to the bulk epoxy resin models created in our earlier study of network formation from smooth topology transfer.[16] Therein, the largest degree of cross-linking achieved so far was $\eta = 93\%$. In Table 1, the degree of cross-linking η, density ρ, glass transition temperature T_g, formation energy $Q_{formation}$, and mechanical properties of this system are compared for both force-fields to confirm that our reactive FF reasonably reproduces the data collected from OPLS-AA with fixed topology. While the computed properties are well in the range expected for epoxy resins, the yet observable differences between the OPLS-AA and the reactive FF indicate the effect of different modeling of the intramolecular angle terms. Arguably, when comparing either of these model λ's to the experimental λ_{exp}, the most important issue still lies within the degree of cross-linking. While $\eta = 93\%$ constitutes the best value in terms of modeling the curing process reported so far, this is still 5−7% off from state-of-the-art epoxy resins in industrial use. In what follows, we hence focus on our new model $\lambda_{large}^{reactive}$ which closes this gap by featuring $\eta = 98\%$.

Modeling Deformation and Fracture

The cured epoxy models combined with the reactive force-field constitute widely applicable starting points to molecular simulations of mechanical testing. Apart from the already discussed elastic properties, this also includes bond dissociation and reorganization—hence enabling plastic deformation and fracture analyses. In the following, we describe MD

Table 1. Comparison of Curing Properties and Elastic Constants as Obtained from Experiment, OPLS-AA with Fixed Topology (Reference Based on QM/MM Modeling of the Linking Reactions[16]) and the Newly Created Reactive Model[a]

	λ_{exp}	λ_{ref}^{OPLS}	$\lambda_{switch}^{reactive}$	$\lambda_{cured}^{reactive}$	$\lambda_{large}^{reactive}$
BFDGE:DEDTA	$2{:}1 \times \infty$	256:128	256:128	256:128	2048:1024
$\eta/\%$	99^b	93	93	98	98
$\rho/\text{g cm}^{-3}$	1.2^c	1.05	1.13	1.16	1.16
T_g/K	$440-470^d$	484	432	446	439
$Q_{formation}/\text{J g}^{-1}$	418 ± 7^e	409	399	451	459
$\langle Y \rangle/\text{GPa}$	$2.5-3.0^f$	3.2 ± 0.3	2.6 ± 0.4	2.6 ± 0.2	2.6 ± 0.3
$\langle G \rangle/\text{GPa}$	0.95^g	1.1 ± 0.1	0.9 ± 0.1	1.0 ± 0.1	0.9 ± 0.1
$\langle K \rangle/\text{GPa}$	2.9^g	3.6 ± 0.4	3.6 ± 0.4	4.0 ± 0.3	4.0 ± 0.3
$\langle \nu \rangle$	0.35^h	0.38 ± 0.05	0.43 ± 0.09	0.38 ± 0.03	0.41 ± 0.03

[a]For the latter, three systems λ are characterized, as indicated by *switch* (geometry of the reference model for direct comparison), *cured* (same model size as the reference, but fully cured using the reactive FF model), and the larger system (*large*) used for the deformation and fracture simulations. [b]Cai et al.[18] [c]EPIKOTE Resin 862.[33] [d]Tao et al.[34] [e]Meißner et al.[16] [f]Bajpai et al.[35] [g]Kallivokas et al.[36] [h]Littell et al.[37]

simulations of uniaxial tensile testing to demonstrate the analyses of the molecular mechanisms involved. For this purpose, we chose the largest of our model systems, $\lambda_{large}^{reactive}$, with a cross-linking degree of 98% and relaxed at 300 K and 1 atm as the starting point. Applying 3D periodic boundary conditions, one axis s is gradually elongated by applying linear scaling of the atomic coordinates before each MD step. This is followed by the actual MD step which maintains the elongation Δs, whereas all other degrees of freedom are allowed to relax. This relaxation includes the volume of the simulation box by subjecting the cell vectors normal to the pulling direction to a 2D barostat imposing 1 atm pressure[27] and the damping of excess energy by maintaining 300 K throughout the deformation and fracture runs. Our analysis of the deformation and fracture behavior is based on a series of three different strain rates, namely, $\dot{\varepsilon} = 10^{10}, 10^9,$ and 10^8 s^{-1} which corresponds to, $\Delta\dot{s} = 84, 8.4,$ and 0.84 m/s, respectively.

Figure 5 shows a sequence of snapshots from our MD runs (illustrated for the slowest pulling rate), whereas stress−strain diagrams and energy profiles are provided for all rates in Figure 6 and Figure 8, respectively. The epoxy models exhibit distinct regimes of elastic/plastic deformation, void nucleation, and fracture. Near $\varepsilon = 0$, we find the stress−strain diagram to approximately follow the idealized elastic $\sigma = Y\cdot\varepsilon$ behavior (with $Y = 2.6$ GPa; see also Table 1). However, already at $\varepsilon > 0.01$ we observe systematic deviation from linear stress increase. Subject to the deformation rate, this nonlinear elastic regime shifts into plastic deformation behavior at $\varepsilon_{yield} = 0.05-0.09$ (identified from the kink in the stress−strain curve, Figure 6) with 0.05 referring to the lowest strain rate. To confirm the assessment of the yield point, we performed an additional tensile testing run (focusing on the range $\varepsilon = 0-0.2$) using $\dot{\varepsilon} = 10^7 \text{ s}^{-1}$, and the observed yield point is plotted as a function of the strain rate in the inset of Figure 6. Plastic deformation is accompanied by reorganizations of the polymer network which was found as (i) unwinding/sliding of loops without (yet) breaking bonds and (ii) rearrangement of epoxy bonds, that is, the cleavage of nearby links, followed by crosswise binding of new partners such that the overall degree of cross-linking remains constant. An illustration of the sliding of different strands of the epoxy network is shown in Figure 7. While this type of plastic deformation mechanism may be directly observed from inspecting the trajectories of the $\dot{\varepsilon} = 10^7-10^{10} \text{ s}^{-1}$ runs, we argue that the reorganization of the epoxy bond network occurs on much longer time scales. We therefore picked a series of snapshots from the tensile testing and
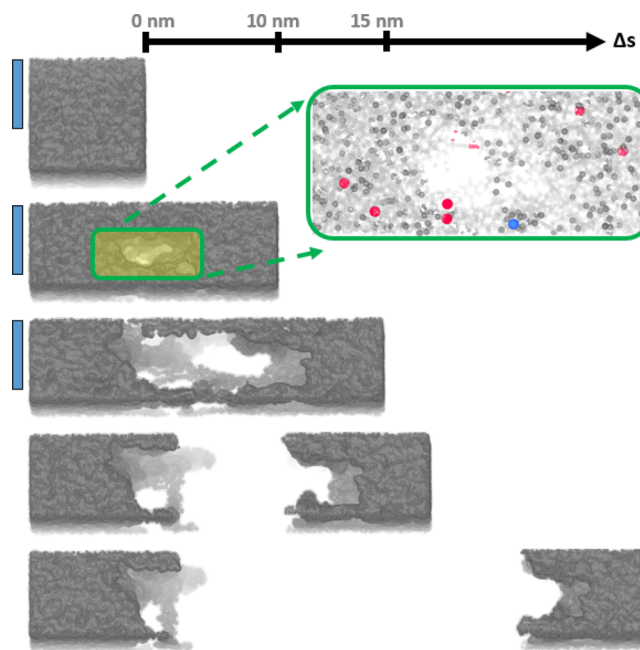

Figure 5. Snapshots taken from the MD run of tensile testing (at 300 K and 1 atm) using the lowest pulling rate ($\Delta\dot{s} = 0.84$ m/s). The blue scale bars indicate 5 nm. Upon model elongation beyond the elastic regime, the system dimensions normal to the pulling direction s reduce by up to 30%. The inset highlights void nucleation ($s = 10$ nm) using a color code to mark the C atoms of unchanged connectivity (gray balls), and epoxy bonds that were broken (red) or reorganized in favor of novel epoxy links (blue).

explored long-termed relaxation at constant model elongation Δs. This indeed led to the identification of epoxy network reorganization in terms of bond rearrangement while maintaining the overall degree of cross-linking as discussed later. The full stress−strain and energy profiles of the tensile testing runs are shown as functions of Δs in Figure 8. In principle, the engineering strain may be calculated from $\varepsilon = \Delta s/l_0$ with $l_0 = 8.4$ nm; however, because of the small size of our simulation model in contrast to epoxy samples in the experiments, comparability of the engineering strain values is arguably very limited once the model is elongated beyond the elastic regime. Trajectory analyses as functions of model elongation Δs included the monitoring of the overall cross-linking degree η and the discrimination of bond reorganization which, for the sake of comparability, we also denote as
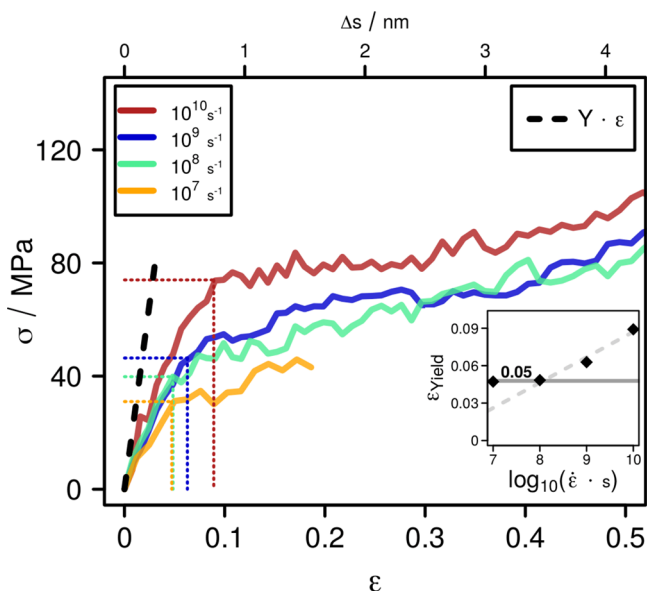
Figure 6. Close-up of the stress–strain profiles highlighting the transition from (nonlinearly) elastic to plastic deformation. The yield point identification is based on the kinks in the curves as indicated by the dotted lines. The resulting $\varepsilon_{\text{yield}}$ is also plotted as a function of the strain rate using a logarithmic scale.
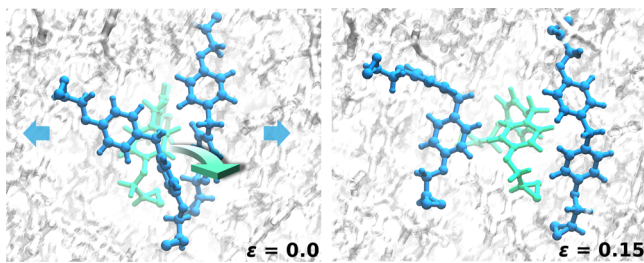

Figure 7. Sliding of three exemplary polymer strands as observed during the early stage of plastic deformation. The blue arrows indicate the pulling direction of the tensile testing, whereas the green arrow highlights an intercalation type motion.

percentages of all epoxy moieties η_{reorg}. On this basis, we relate fracture to the net loss of epoxy bonds which was observed from $\Delta s > 5$ nm (Figure S4). Upon further bond dissociation, void growth and coalescence leads to a maximum in the stress–strain profiles near $\Delta s = 10$ nm, and roughly constant stress before rupture which was found close to $\Delta s = 15$ nm. It is furthermore educative to compare the mechanical work needed for tensile testing with the potential energy as computed from the atomic interactions. During elastic deformation, the mechanical work is fully transferred into potential energy. However, significant deviation of the two curves is already observed from $\Delta s > 2$ nm. This stems from the unwinding and slipping of polymer segments during plastic deformation. Likewise, the dissociation of bonds during fracture leads to the transfer of potential energy into heat. Both of these relaxation processes hence lead to an increase in kinetic energy, which is however damped by the thermostat that maintains 300 K throughout the tensile testing runs. As a consequence, the deviation of mechanical work and potential energy indicates the heat formation experienced during plastic deformation and fracture. A series of snapshots taken from the tensile testing run at the lowest strain rate explored is

illustrated in Figure 5. During elastic deformation, we find the overall volume of the simulation cell roughly conserved, and also during plastic deformation, we find the epoxy models to contract by up to 30% along the dimensions normal to the elongation direction. This lateral contraction behavior is arrested upon void nucleation and fracture of the system. While the onset of epoxy bond dissociation is observed at $\Delta s = 5$ nm, well-defined voids are best seen for larger elongations. The inset in in Figure 5 highlights the epoxy network at $\Delta s = 10$ nm using a color code to mark the cleavage of epoxy bonds and newly formed links in the network, respectively. Analogous illustrations of bond cleavage and/or reorganization during later stages of void growth/coalescence and material failure are provided in the Supporting Information S2. The observed modification of the network of epoxy links is drastically dependent on the strain rate applied in our tensile testing simulations. On one hand, this is reflected by the different reduction of the overall degree of cross-linking upon fracture (Table 2). Moreover, in Figure 9 we are highlighting the evolution of samples depicted from the tensile runs after elongation by $\Delta s = 10$. In particular, for the fastest pulling rate, we find that allowing an additional 10 ns relaxation at constant Δs leads to substantial network reorganization. However, the slowest strain rate explored in our tensile testing runs also exhibits incomplete relaxation. While the computational limitations inherent to molecular dynamics simulations hinder direct application of the strain rates used in common experiments, we can still employ the relaxation kinetics of the constant-elongation runs to estimate the plastic deformation and fracture characteristics at slower model elongation. For this purpose, we changed to pull-and-hold simulations and took a series of snapshots from the tensile-testing runs to explore nanosecond-scale relaxation dynamics at constant strain as discussed in detail in SI section S4. For the decay of stress $\sigma_{\Delta s=\text{const}}$ (t), we assume first-order kinetics of the epoxy network reorganization and hence performed exponential fits to obtain extrapolated values for the stress at infinite relaxation time. On this basis, we produced profiles of $\sigma_{\Delta s=\text{const}}$ $(t \to \infty)$ as a function of Δs which we take as the quasi-static stress–strain diagram (see SI section S4). Based on these fits, the asymptotic stress values as plotted in Figure 8 (gray curve in the upper panel) may be considered approximations to quasi-static conditions. Indeed, for each of the tensile testing runs, the stress profiles extrapolated to the quasi-static limit converge to substantially lower ultimate tensile stress—which is found to be roughly 84 MPa (detailed discussion is provided at the end of this section). Likewise, we use quasi-static extrapolation for the discrimination of epoxy bond reorganization (plastic deformation without net reduction of the cross-linking degree) and bond rupture upon fracture as indicated in Figure 8 and summarized in Table 2. Additional molecular dynamics runs were also performed for assessing the damage induced by plastic deformation. Again, a selection of snapshots was depicted from the tensile testing runs; however, now employed as starting points for reversing the elongation at the same strain rate, namely, by application of $-\Delta \dot{s}$. In each of these runs, full reversal to $\Delta s = 0$ was investigated while monitoring the potential energy and changes in the epoxy network (Figure S7). On this basis, we identified the minimum of the potential energy min $(E_{\Delta s\to 0}^{\text{pot}})$ for each reverse run (Table 2). The profile of min $(E_{\Delta s\to 0}^{\text{pot}})$ is shown as a function of the elongation Δs from which the reverse runs were started in Figure 8 (gray curve in the lower panel), whereas the locations
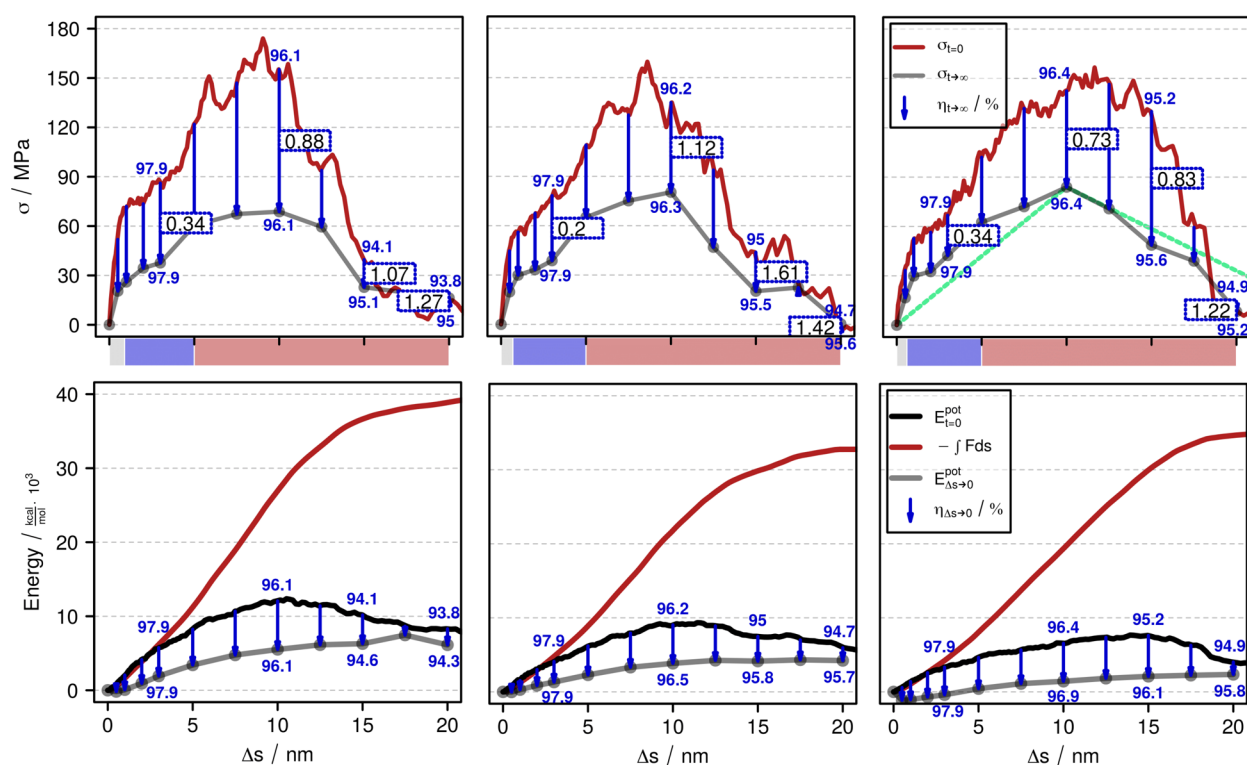
Figure 8. Tensile tests performed at different pulling rates (left to right: $\Delta \dot{s}$ = 84, 8.4, and 0.84 m/s). The upper panel shows the stress profiles upon model elongation (red curve) and after additional relaxation while keeping Δs constant (gray), respectively. The elastic and plastic regimes in the stress–strain diagram are indicated by gray and blue bars, while void nucleation and fracture is indicated in red, respectively. During quasi-static relaxation, we monitor the absolute change in epoxy cross-linking (percentages denoted in blue) and the fraction of reorganized links (shown as flags). The lower panel illustrates the mechanical work (red curve) and the potential energy of the epoxy model (black) during tensile testing. Moreover, for a series of snapshots we reversed the pulling using the same rate as during the tensile tests. This leads to (partial) restoring of the cross-linking (numbers next to blue arrows) and the potential energy. The profile (gray) of the resulting minimum energy configurations indicates the damage energy stemming from plastic deformation and void formation. The zero point of the potential energy profiles is chosen as that of the pristine simulation model prior to tensile testing.

Table 2. Characterization of Snapshots of Various Elongation Δs Taken along the Tensile Testing Run Using $\dot{\epsilon} = 10^8$ s^{-1a}

Δs/nm	$\eta_{t=0}$/%	$n_{t\to\infty}^{reorg}$/%	$\sigma_{t=0}$/MPa	$\sigma_{t\to\infty}$/MPa	$-\int F\,ds - E_{t=0}^{pot}/\frac{kcal}{mol}\cdot 10^3$	$E_{t=0}^{pot} - \min(E_{\Delta s\to 0}^{pot})$/kcalmol·103	$\Delta s\|_{\min(E_{\Delta s\to 0}^{pot})}$/nm
0	97.9	0	0	0	0	0	0
1	97.9	0.293	52.7	29.9	−0.4	0	0.06
3	97.9	0.342	66.8	42.4	0.5	2.55	0.51
5	97.8	0.439	102	62.6	2.9	4.23	1.10
10	96.4	0.732	142	83.9	14.6	5.15	3.04
15	95.2	0.83	130	48.7	26.4	5.52	3.50
20	94.9	1.22	10.5	8.28	30.5	1.68	2.41

^{a}For each snapshot, the momentary (denoted as $t = 0$) degree of cross-linking $\eta_{t=0}$, stress $\sigma_{t=0}$, and the difference of mechanical work and potential energy $-\int_0^{\Delta s} F\,ds - E_{t=0}^{pot}$ is provided. Data from the relaxation runs at constant Δs is indicated by the suffix $t \to \infty$, while the results of reversing elongation are indicated by $\Delta s \to 0$.

$\Delta s\|_{\min(E_{\Delta s\to 0}^{pot})}$ (cf., Figure S8) of these minima are denoted in Table 2. Within the range of $\epsilon = 0-0.05$ (elastic regime) reversing the deformation leads to (roughly) continuous reduction of the potential energy and eventually full restoration of the sample in terms of both potential energy and model dimensions. On the other hand, models which were strained beyond the yield point before reversing the elongation clearly show persistent damage of the epoxy network. This leads to reshaping $\Delta s\|_{\min(E_{\Delta s\to 0}^{pot})} > 0$ of the simulation system and elevated potential energy $\min(E_{\Delta s\to 0}^{pot}) > 0$ after restoration to zero stress. Upon model elongation beyond $\Delta s = 5$ nm, we observe void nucleation and fracture which implies further

increase of the damage energy $\min(E_{\Delta s\to 0}^{pot})$ and plasticity $\Delta s\|_{\min(E_{\Delta s\to 0}^{pot})}$. This is also reflected by comparing the degree of cross-linking before and after reversing elongation—which indicates that no ($\Delta s < 15$ nm) or at most a minor fraction of ruptured epoxy bonds are recovered (numbers shown in blue at the lower panel of Figure 8). While our coarse-grained, reactive force-field was designed to allow efficient molecular dynamics simulations of deformation and fracture, computational limitations still imply the use of 10 nm scale models and simulation times <100 ns. Indeed, the strain rates applied in tensile testing experiments are by orders of magnitude beyond the reach of direct molecular dynamics simulations. Experimentally, the dependence of deformation and fracture
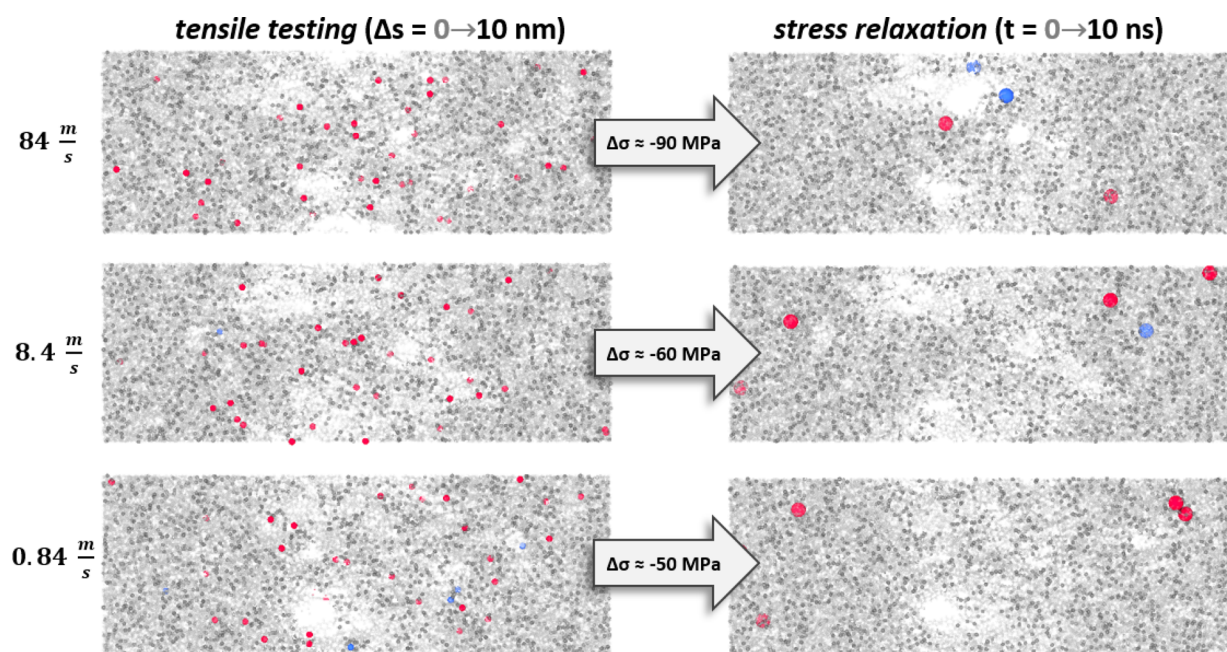
Figure 9. Snapshots taken from the tensile test runs performed at different pulling rates (left column) as contrasted to relaxation runs at constant elongation (right column). For each pulling rate, the snapshots refer to horizontal elongation by $\Delta s = 10$ nm and use a color code to mark C atoms of unchanged connectivity (gray balls), epoxy bonds that were broken (red) or reorganized (blue), each in comparison to the pristine model prior to tensile load. The snapshots shown at the right use the same color code for the C atoms, but now highlighting connectivity changes during the relaxation processes during constant model elongation Δs (with respect to the left column). The scale bar indicates 5 nm.

characteristics as a function of the strain rate was thoroughly elaborated by Littell et al.[37] Scanning $\dot{\varepsilon} = 10^{-5}-10^{-1}$ s^{-1} the yield point was identified near $\epsilon_{\text{yield}} = 0.04$ for all of these experiments. This nicely compares to our estimate of $\epsilon_{\text{yield}} = 0.05$ based on the convergence of various runs using much larger strain rates. Upon model elongation beyond the yield point, the finite size of the simulation system dramatically comes into play. The few nanometers of local elongation needed to allow the slipping of polymer strands or void formation result in engineering strains of $\varepsilon = 0.1-1.5$—which should not be directly compared to the strain applied to macroscopic samples. Our tensile testing runs still provide estimates of the ultimate stress reached before epoxy fracture, which are comparably close to the experimental findings of Littel et al., namely, $\sigma_{\text{ultimate}} = 70-100$ MPa at strain rates of $\dot{\varepsilon} = 10^{-5}-10^{-1}$ s^{-1}, respectively.[37] This is particularly remarkable, as to the best of our knowledge all MD simulation studies of epoxy resin fracture reported so far provided rather drastic overestimation of the ultimate stress. Based on the ReaxFF model, Koo et al. performed ultrafast strain rate ($\dot{\varepsilon} = 10^{13}$ s^{-1}) tensile testing MD runs leading to $\sigma_{\text{ultimate}} = 16-20$ GPa.[23] Moreover, Møller et al. performed in principle classical MD simulations of tensile testing at $\dot{\varepsilon} = 10^{10}$ s^{-1}, however while abruptly switching off bonds that were stretched beyond predefined energy criteria.[9] On that basis, the ultimate stress was found as $5-6$ GPa—which is still a factor of 25 larger than the finding of $\sigma_{\text{ultimate}} = 0.18$ GPa we obtained as the same strain rate. Finally, the hybrid quantum/molecular mechanics tensile testing study of Barr et al., performed at $\dot{\varepsilon} = 10^9$ s^{-1}, also leads to $\sigma_{\text{ultimate}} = 1.5-2$ GPa[13] as compared to $\sigma_{\text{ultimate}} = 0.16$ GPa observed from our model at this strain rate. In turn, our best estimate of the ultimate stress is obtained from the tensile testing runs using (i) the slowest strain rate we could afford with current hardware ($\dot{\varepsilon} = 10^8$ s^{-1}, $\sigma_{\text{ultimate}} = 0.15$ GPa) and (ii) extrapolation of the relaxation kinetics to the quasi-static

approximation (see also SI section S3). On this basis, the ultimate stress for $\dot{\varepsilon} \rightarrow 0$ is obtained as about 84 MPa—which is in reasonably good agreement to the experiment ($\sigma_{\text{ultimate}} = 70$ MPa) at 300 K and vanishing strain rate.[37]

Further fracture-related properties of interest, like fracture toughness, K_{Ic}, and the critical energy release rate G_c are only defined in the presence of a crack. While the entire field of fracture mechanics requires the presence of crack-like defects, this is, strictly speaking, not the case in the presented set of simulations using nanometer-scale systems along with 3D periodic boundaries. The fracture of our samples is the combination of two processes: damage nucleation (which might be seen as crack-nucleation) and damage coalescence (which might be interpreted as crack propagation) and can therefore not be directly interpreted in terms of fracture mechanics. Furthermore, it must be noted that the peak-stress as well as the failure strain strongly depend on the sample, as (i) larger samples can contain larger pre-existing defects, which locally intensify the stress as described by the stress intensity factor K, thereby reducing the required external loading for crack propagation[38] and (ii) the elastically stored energy available for crack propagation scales with the sample dimension along the loading direction, i.e., in computer simulations, larger samples fracture at smaller strains than smaller samples.[39] The results presented in the manuscript can therefore not be directly compared to experimental results. However, our results can be used to inform continuum models like the cohesive zone model (CZM).[40,41] The mathematical theory of equilibrium cracks in brittle fracture,[41,42] which in combination with finite element modeling (FEM) can be used to model fracture experiments. CZM often use traction-separation laws determined from atomistic simulations,[42−44] which use as parameters the work of separation (which can be determined in our case from the integral over the stress

displacement curve), the peak stress, and the displacement at final separation:[43]

$$-\int_0^\infty \sigma_{t \to \infty}(s) \, ds = \frac{1}{2}\sigma_{\text{ultimate}} \cdot \Delta s_{\text{final separation}} \qquad (1)$$

In other terms, a bilinear approximation is used to describe the work of separation by a stress−elongation triangle (green lines in Figure 8) defined by ultimate stress at critical elongation and zero stress at $\Delta s = 0$ and $\Delta s_{\text{final separation}}$, respectively. Using the extrapolated stress estimates for vanishing strain rate, the work of separation was found as 0.1 J/m². Combined with $\sigma_{\text{ultimate}} =$ 84 MPa at $\Delta s_{\text{crit}} = 10$ nm, this leads to $\Delta s_{\text{final separation}} = 32$ nm as suggested inputs for continuum models of epoxy fracture.

4. CONCLUSIONS

In conclusion, we outlined a molecular mechanics model for BFDGE and DETDA based thermosetting polymers which includes the formation and dissociation of epoxy bonds without the need of (further) quantum mechanical calculations. In combination with a previously developed algorithm for the identification of stepwise network linking featuring exothermic reaction steps,[16] our reactive force-field enables the identification of realistic epoxy models of atomic resolution. The quality of the resulting molecular simulation systems is demonstrated by the degree of cross-linking, heat of formation, glass transition temperature, density, and the elastic properties—which were all found in excellent agreement with experimental characterization studies taken from the literature. Moreover, the obtained model provides a playground for investigating molecular processes that account for the plastic deformation and fracture behavior of the cured polymer. To demonstrate this, we performed tensile testing runs, including reversal of material elongation and flanked by molecular dynamics characterization of snapshots picked from the tensile testing runs and subjected to relaxation at constant strain. Using such combined evidence from different simulation setups allows us to somewhat reconcile for the still rather limited time and length scales accessible to current hardware. In particular, our models provide realistic values for the yield strain and the ultimate stress which so far have been drastically overestimated by previous molecular simulation studies. The outlined modeling of both epoxy curing and the mechanical characterization is widely transferable, and yet ongoing studies are dedicated to exploring the role of boundaries and interfaces in finite epoxy samples and composite systems, respectively.

ASSOCIATED CONTENT

Supporting Information

The Supporting Information is available free of charge at https://pubs.acs.org/doi/10.1021/acspolymersau.1c00016.

Details on the reactive force-field (S1), tensile testing (S2), constant strain relaxation (S3) and strain reversal (S4) (PDF)

AUTHOR INFORMATION

Corresponding Author

Dirk Zahn − Department of Chemistry and Pharmacy, Computer Chemistry Center, Friedrich-Alexander-Universität Erlangen-Nürnberg, Erlangen 91052, Germany; orcid.org/0000-0002-4303-3422; Email: dirk.zahn@fau.de

Authors

Julian Konrad − Department of Chemistry and Pharmacy, Computer Chemistry Center, Friedrich-Alexander Universität Erlangen-Nürnberg, Erlangen 91052, Germany

Robert H. Meißner − Institute of Polymers and Composites, Hamburg University of Technology, Hamburg 21073, Germany; Helmholtz-Zentrum Hereon, Institute of Surface Science, Geesthacht 21502, Germany; orcid.org/0000-0003-1926-114X

Erik Bitzek − Department of Materials Science and Engineering, Institute I, Friedrich-Alexander-Universität Erlangen-Nürnberg, Erlangen 91052, Germany

Complete contact information is available at:
https://pubs.acs.org/10.1021/acspolymersau.1c00016

Notes

ACKNOWLEDGMENTS

REFERENCES

(1) Schlack, P. IG-Farbenindustrie, Preparation of Polyamides; 1938. German Patent 676 117; US Patent US 2,136,928.

(2) Lee, H.; Neville, K. Handbook of Epoxy Resins; McGraw-Hill: New York, 1967.

(3) May, C. Epoxy Resins - Chemistry and Technology, 2nd ed.; CRC Press: Boca Raton, FL, 1987.

(4) Ellis, B., Ed. Chemistry and Technology of Epoxy Resins; Springer: Netherlands, 1993.

(5) Brown, R.; Brown, A. E. Epoxy Basics - Working With Epoxy Cleanly & Efficiently; Createspace Independent Pub, 2013.

(6) Heilen, W.; Herrwerth, S. Silicone Resins and Their Combinations; Vincentz Network: Hannover, 2014.

(7) Varshney, V.; Patnaik, S. S.; Roy, A. K.; Farmer, B. L. A Molecular Dynamics Study of Epoxy-Based Networks: Cross-Linking Procedure and Prediction of Molecular and Material Properties. Macromolecules 2008, 41, 6837−6842.

(8) Nouri, N.; Ziaei-Rad, S. A Molecular Dynamics Investigation on Mechanical Properties of Cross-Linked Polymer Networks. Macromolecules 2011, 44, 5481−5489.

(9) Moller, J. C.; Barr, S. A.; Schultz, E. J.; Breitzman, T. D.; Berry, R. J. Simulation of Fracture Nucleation in Cross-Linked Polymer Networks. JOM 2013, 65, 147−167.

(10) Shokuhfar, A.; Arab, B. The effect of cross linking density on the mechanical properties and structure of the epoxy polymers: molecular dynamics simulation. J. Mol. Model. 2013, 19, 3719−3731.

(11) Sundararaghavan, V.; Kumar, A. Molecular dynamics simulations of compressive yielding in cross-linked epoxies in the context of Argon theory. Int. J. Plast. 2013, 47, 111−125.

(12) Xin, D. R.; Han, Q. Molecular dynamics study on the tensile deformation of cross-linking epoxy resin. J. Mol. Model. 2015, 21, 1 DOI: 10.1007/s00894-014-2567-z.

(13) Barr, S. A.; Kedziora, G. S.; Ecker, A. M.; Moller, J. C.; Berry, R. J.; Breitzman, T. D. Bond breaking in epoxy systems: A combined QM/MM approach. J. Chem. Phys. 2016, 144, 244904.

(14) Okabe, T.; Oya, Y.; Tanabe, K.; Kikugawa, G.; Yoshioka, K. Molecular dynamics simulation of crosslinked epoxy resins: Curing and mechanical properties. Eur. Polym. J. 2016, 80, 78−88.

(15) Laurien, M.; Demir, B.; Büttemeyer, H.; Herrmann, A. S.; Walsh, T. R.; Ciacchi, L. C. Atomistic Modeling of the Formation of a Thermoset/Thermoplastic Interphase during Co-Curing. *Macromolecules* **2018**, *51*, 3983−3993.

(16) Meißner, R. H.; Konrad, J.; Boll, B.; Fiedler, B.; Zahn, D. Molecular Simulation of Thermosetting Polymer Hardening: Reactive Events Enabled by Controlled Topology Transfer. *Macromolecules* **2020**, *53*, 9698−9705.

(17) Gartner, T. E.; Jayaraman, A. Modeling and Simulations of Polymers: A Roadmap. *Macromolecules* **2019**, *52*, 755−786.

(18) Cai, H.; Li, P.; Sui, G.; Yu, Y.; Li, G.; Yang, X.; Ryu, S. Curing kinetics study of epoxy resin/flexible amine toughness systems by dynamic and isothermal DSC. *Thermochim. Acta* **2008**, *473*, 101−105.

(19) Bandyopadhyay, A.; Valavala, P. K.; Clancy, T. C.; Wise, K. E.; Odegard, G. M. Molecular modeling of crosslinked epoxy polymers: The effect of crosslink density on thermomechanical properties. *Polymer* **2011**, *52*, 2445−2452.

(20) Li, C.; Strachan, A. Molecular simulations of crosslinking process of thermosetting polymers. *Polymer* **2010**, *51*, 6058−6070.

(21) Tow, G. M.; Maginn, E. J. Cross-Linking Methodology for Fully Atomistic Models of Hydroxyl-Terminated Polybutadiene and Determination of Mechanical Properties. *Macromolecules* **2021**, *54*, 4488−4496.

(22) Senftle, T. P.; Hong, S.; Islam, M. M.; Kylasa, S. B.; Zheng, Y.; Shin, Y. K.; Junkermeier, C.; Engel-Herbert, R.; Janik, M. J.; Aktulga, H. M.; Verstraelen, T.; Grama, A.; van Duin, A. C. T. The ReaxFF reactive force-field: development, applications and future directions. *npj Computational Materials* **2016**, *2*, 1 DOI: 10.1038/npjcompumats.2015.11.

(23) Koo, B.; Subramanian, N.; Chattopadhyay, A. Molecular dynamics study of brittle fracture in epoxy-based thermoset polymer. *Composites, Part B* **2016**, *95*, 433−439.

(24) Vashisth, A.; Ashraf, C.; Zhang, W.; Bakis, C. E.; van Duin, A. C. T. Accelerated ReaxFF Simulations for Describing the Reactive Cross-Linking of Polymers. *J. Phys. Chem. A* **2018**, *122*, 6633−6642.

(25) Beyer, M. K. The mechanical strength of a covalent bond calculated by density functional theory. *J. Chem. Phys.* **2000**, *112*, 7307−7312.

(26) Frisch, M. J. et al. *Gaussian 16*, Revision C.01.; Gaussian Inc.: Wallingford, CT, 2016.

(27) Plimpton, S. Fast Parallel Algorithms for Short-Range Molecular Dynamics. *J. Comput. Phys.* **1995**, *117*, 1−19.

(28) Zahn, D.; Schilling, B.; Kast, S. M. Enhancement of the Wolf Damped Coulomb Potential: Static, Dynamic, and Dielectric Properties of Liquid Water from Molecular Simulation. *J. Phys. Chem. B* **2002**, *106*, 10725−10732.

(29) Humphrey, W.; Dalke, A.; Schulten, K. VMD - Visual Molecular Dynamics. *J. Mol. Graphics* **1996**, *14*, 33−38.

(30) RStudio Team, *RStudio: Integrated Development Environment for R. RStudio*; PBC: Boston, MA, 2020.

(31) The GIMP Development Team, *GIMP*, version 2.10.12.

(32) Dickinson, J. T.; Donaldson, E. E.; Park, M. K. The emission of electrons and positive ions from fracture of materials. *J. Mater. Sci.* **1981**, *16*, 2897−2908.

(33) *EPICOTE Resin 862*; Hexion, 2009.

(34) Tao, K.; Yang, S.; Grunlan, J. C.; Kim, Y.-S.; Dang, B.; Deng, Y.; Thomas, R. L.; Wilson, B. L.; Wei, X. Effects of carbon nanotube fillers on the curing processes of epoxy resin-based composites. *J. Appl. Polym. Sci.* **2006**, *102*, 5248−5254.

(35) Bajpai, A.; Alapati, A.; Klingler, A.; Wetzel, B. Tensile Properties, Fracture Mechanics Properties and Toughening Mechanisms of Epoxy Systems Modified with Soft Block Copolymers, Rigid TiO2 Nanoparticles and Their Hybrids. *Journal of Composites Science* **2018**, *2*, 72.

(36) Kallivokas, S. V.; Sgouros, A. P.; Theodorou, D. N. Molecular dynamics simulations of EPON-862/DETDA epoxy networks: structure, topology, elastic constants, and local dynamics. *Soft Matter* **2019**, *15*, 721−733.

(37) Littell, J. D.; Ruggeri, C. R.; Goldberg, R. K.; Roberts, G. D.; Arnold, W. A.; Binienda, W. K. Measurement of Epoxy Resin Tension, Compression, and Shear Stress-Strain Curves over a Wide Range of Strain Rates Using Small Test Specimens. *Journal of Aerospace Engineering* **2008**, *21*, 162−173.

(38) Lawn, B. *Fracture of Brittle Solids*; Cambridge University Press, 1993.

(39) Elsner, B. A. M.; Müller, S. Size effects and strain localization in atomic-scale cleavage modeling. *J. Phys.: Condens. Matter* **2015**, *27*, 345002.

(40) Dugdale, D. Yielding of steel sheets containing slits. *J. Mech. Phys. Solids* **1960**, *8*, 100−104.

(41) Barenblatt, G. *Advances in Applied Mechanics*; Elsevier, 1962; pp 55−129.

(42) Möller, J. J.; Bitzek, E.; Janisch, R.; ul Hassan, H.; Hartmaier, A. Fracture ab initio: A force-based scaling law for atomistically informed continuum models. *J. Mater. Res.* **2018**, *33*, 3750−3761.

(43) Tahir, A. M.; Janisch, R.; Hartmaier, A. Ab initiocalculation of traction separation laws for a grain boundary in molybdenum with segregated C impurites. *Modell. Simul. Mater. Sci. Eng.* **2013**, *21*, 075005.

(44) Stewart, J. A.; Spearot, D. E. Atomistic simulations of nanoindentation on the basal plane of crystalline molybdenum disulfide (MoS2). *Modell. Simul. Mater. Sci. Eng.* **2013**, *21*, 045003.